

Carbon nanodots: Opportunities and limitations to study their biodistribution at the human lung epithelial tissue barrier

Estelle Durantie, Hana Barosova, Barbara Drasler, Laura Rodriguez-Lorenzo, Dominic A. Urban, Dimitri Vanhecke, Dedy Septiadi, Liliane Hirschi-Ackermann, Alke Petri-Fink, and Barbara Rothen-Rutishauser

Citation: *Biointerphases* **13**, 06D404 (2018); doi: 10.1116/1.5043373

View online: <https://doi.org/10.1116/1.5043373>

View Table of Contents: <https://avs.scitation.org/toc/bip/13/6>

Published by the [American Vacuum Society](#)

ARTICLES YOU MAY BE INTERESTED IN

[Engineered systems to study the synergistic signaling between integrin-mediated mechanotransduction and growth factors \(Review\)](#)

Biointerphases **13**, 06D302 (2018); <https://doi.org/10.1116/1.5045231>

[Analysis of the Myc-induced pancreatic \$\beta\$ cell islet tumor microenvironment using imaging ToF-SIMS](#)

Biointerphases **13**, 06D402 (2018); <https://doi.org/10.1116/1.5038574>

[Nitric oxide-mediated fibrinogen deposition prevents platelet adhesion and activation](#)

Biointerphases **13**, 06E403 (2018); <https://doi.org/10.1116/1.5042752>

[Exploring the anomalous cytotoxicity of commercially-available poly\(N-isopropyl acrylamide\) substrates](#)

Biointerphases **13**, 06D406 (2018); <https://doi.org/10.1116/1.5045142>

[Nanostructured biomedical selenium at the biological interface \(Review\)](#)

Biointerphases **13**, 06D301 (2018); <https://doi.org/10.1116/1.5042693>

[Tunability of liquid-infused silicone materials for biointerfaces](#)

Biointerphases **13**, 06D401 (2018); <https://doi.org/10.1116/1.5039514>

Spectra
Simplified

Plot, compare, and validate
your data with just a click

eSpectra:
surface science

SEE HOW IT WORKS



Carbon nanodots: Opportunities and limitations to study their biodistribution at the human lung epithelial tissue barrier

Estelle Durantie,^{1,a)} Hana Barosova,^{1,a)} Barbara Drasler,¹ Laura Rodriguez-Lorenzo,^{1,2} Dominic A. Urban,¹ Dimitri Vanhecke,¹ Dedy Septiadi,¹ Liliane Hirschi-Ackermann,¹ Alke Petri-Fink,^{1,3} and Barbara Rothen-Rutishauser^{1,b)}

¹Adolphe Merkle Institute, University of Fribourg, Chemin des Verdiers 4, CH-1700 Fribourg, Switzerland

²Water Quality Group, Water4Environment Unit, Department of Life Sciences, International Iberian Nanotechnology Laboratory, Av. Mestre José Veiga, 4715-330 Braga, Portugal

³Chemistry Department, University of Fribourg, Chemin du Musée 9, CH-1700 Fribourg, Switzerland

(Received 8 June 2018; accepted 15 August 2018; published 11 September 2018)

Inhalation of combustion-derived ultrafine particles ($\leq 0.1 \mu\text{m}$) has been found to be associated with pulmonary and cardiovascular diseases. However, correlation of the physicochemical properties of carbon-based particles such as surface charge and agglomeration state with adverse health effects has not yet been established, mainly due to limitations related to the detection of carbon particles in biological environments. The authors have therefore applied model particles as mimics of simplified particles derived from incomplete combustion, namely, carbon nanodots (CNDs) with different surface modifications and fluorescent properties. Their possible adverse cellular effects and their biodistribution pattern were assessed in a three-dimensional (3D) lung epithelial tissue model. Three different CNDs, namely, nitrogen, sulfur codoped CNDs (*N,S*-CNDs) and nitrogen doped CNDs (*N*-CNDs-1 and *N*-CNDs-2), were prepared by microwave-assisted hydrothermal carbonization using different precursors or different microwave systems. These CNDs were found to possess different chemical and photophysical properties. The surfaces of nanodots *N*-CNDs-1 and *N*-CNDs-2 were positively charged or neutral, respectively, arguably due to the presence of amine and amide groups, while the surfaces of *N,S*-CNDs were negatively charged, as they bear carboxylic groups in addition to amine and amide groups. Photophysical measurements showed that these three types of CNDs displayed strong photon absorption in the UV range. Both *N*-CNDs-1 and *N,S*-CNDs showed weak fluorescence emission, whereas *N*-CNDs-2 showed intense emission. A 3D human lung model composed of alveolar epithelial cells (A549 cell line) and two primary immune cells, i.e., macrophages and dendritic cells, was exposed to CNDs via a pseudo-air-liquid interface at a concentration of $100 \mu\text{g/ml}$. Exposure to these particles for 24 h induced no harmful effect on the cells as assessed by cytotoxicity, cell layer integrity, cell morphology, oxidative stress, and proinflammatory cytokines release. The distribution of the CNDs in the lung model was estimated by measuring the fluorescence intensity in three different fractions, e.g., apical, intracellular, and basal, after 1, 4, and 24 h of incubation, whereby reliable results were only obtained for *N*-CNDs-2. It was shown that *N*-CNDs-2 translocate rapidly, i.e., $>40\%$ in the basal fraction within 1 h and almost 100% after 4 h, while ca. 80% of the *N*-CNDs-1 and *N,S*-CNDs were still located on the apical surface of the lung cells after 1 h. This could be attributed to the agglomeration behavior of *N*-CNDs-1 or *N,S*-CNDs. The surface properties of the *N*-CNDs bearing amino and amide groups likely induce greater uptake as *N*-CNDs could be detected intracellularly. This was less evident for *N,S*-CNDs, which bear carboxylic acid groups on their surface. In conclusion, CNDs have been designed as model systems for carbon-based particles; however, their small size and agglomeration behavior made their quantification by fluorescence measurement challenging. Nevertheless, it was demonstrated that the surface properties and agglomeration affected the biodistribution of the particles at the lung epithelial barrier *in vitro*. © 2018 Author(s). All article content, except where otherwise noted, is licensed under a Creative Commons Attribution (CC BY) license (<http://creativecommons.org/licenses/by/4.0/>). <https://doi.org/10.1116/1.5043373>

I. INTRODUCTION

Epidemiological studies conducted over the last two decades have shown a positive correlation between the level

of particulate air pollution and increased adverse health effects,^{1–3} including increased pulmonary diseases^{4,5} as well as a rise in the number of deaths from cardiovascular disease.^{6–9} The exact causal connection between air pollution—including particles derived from incomplete combustion processes such as ultrafine particles (UFPs), i.e., those smaller than 100 nm in diameter—and adverse health effects

^{a)}E. Durantie and H. Barosova contributed equally to this work.

^{b)}Author to whom correspondence should be addressed: barbara.rothen@unifr.ch

is still not fully understood; however, certain molecular and cellular mechanisms are generally assumed to play a key role. In addition, the translocation of UFPs across the lung barrier into the blood stream is also difficult to assess with traditional carbon-based particles. To date, there is only one study that describes a rapid and significant translocation of inhaled carbonaceous nanoparticles to the systemic circulation and other extrapulmonary organs,¹⁰ whereas other similar studies detected only a low degree of translocation of carbonaceous nanoparticles.^{11,12} Studies of Nemmar *et al.*¹⁰ and Mills *et al.*¹¹ have provided a convincing argument that the particle translocation observed was mainly a result of the translocation of soluble pertechnate used as a detection signal that had been cleaved from the carbonaceous particles. It is therefore currently accepted that the degree to which inhaled UFPs translocate into the circulation is rather small; however, cumulative effect data for this translocation are lacking. A major fraction of UFPs is composed of a carbonaceous core resulting from incomplete combustion or high temperature processes. The major sources of these pollutants are the combustion of fossil fuels and common human activities, such as cooking, candle burning, cigarette smoke, and printing.¹³ The unique properties of UFPs (i.e., their small size and large reactive surface area) can make them particularly harmful to the lung and other organs.¹⁴ Due to their small size, UFPs diffuse deeply into the lung^{15,16} and upon deposition in the alveolar region, interact locally with lung cells or translocate across the lung barrier, thus reaching the blood or lymphatic circulation. Controlled human exposures with elemental carbon UFPs have shown adverse effects on the lungs and cardiovascular system.¹³ On the other hand, the organic content of UFPs has been intrinsically correlated with the induction of higher oxidative stress.¹⁷

It is important to establish the relationship between the structure and composition of inhaled ultrafine carbon particles and their adverse health effects in order to clearly identify the hazardous components. We have therefore applied model carbon particles to study the biodistribution upon exposure onto the three-dimensional (3D) lung cell coculture model. The particles chosen as model are carbon nanodots (CNDs), which can be synthesized, tuned with respect to their surface chemistry and agglomeration behavior, and are furthermore less toxic than quantum dots.¹⁸ In particular, CNDs were chosen as the particle models due to their unique properties: (i) their reliable mimicry of ultrafine airborne particles, (ii) their particularly small size (<10 nm), (iii) their controllable surface chemistry, and (iv) their fluorescent properties. CNDs are formed of a carbon core composed of paracrystalline domains, i.e., carbon sp^2 domains with sp^3 defects while their surface is mainly composed of sp^3 carbon atoms and functional groups. This structure confers interesting optical properties such as strong light absorption in the UV region and photoluminescence in the blue-green optical window.¹⁹ Among the various routes to synthesize CNDs, the combustion of carbon precursors is a very interesting approach given its similarity to the carbonaceous airborne particles generation, as well as the possibility of surface functionalization.²⁰

In the following study, we have explored the biodistribution of different CNDs across a lung barrier model after different exposure time points, i.e., 1, 4, and 24 h. Three CNDs with different properties were prepared, all of which bear nitrogen functional groups at the surface; **N-CNDs-1**, which are strongly agglomerated; **N-CNDs-2**, which are highly hydrophilic; and **N,S-CNDs** bearing thiol and carboxylic groups, which are negatively charged. Their biodistribution was analyzed on the 3D lung model developed by Rothen-Rutishauser *et al.*,²¹ composed of human lung alveolar cells (A549), primary human monocyte-derived macrophages (MDM), and monocyte-derived dendritic cells (MDDC). The cells were exposed to CNDs at a concentration of 100 μ g/ml under pseudo-air-liquid interface [pseudo-air-liquid interface (ALI)] conditions. Cytotoxicity, oxidative stress, and proinflammation were assessed after 24 h. CNDs' fractions were monitored after 1, 4, and 24 h by fluorescence measurements, i.e., in the small volume of added phosphate-buffered saline (PBS) solution or attached to the cells at the apical side, in the cellular fraction, and in the medium from the basal side.

II. EXPERIMENT

All the chemicals and reagents were purchased from Sigma-Aldrich (Switzerland) unless otherwise specified. All cell culture reagents were purchased from Gibco, Thermo Fisher Scientific (Switzerland), unless otherwise specified.

MilliQ water (H_2O) was used in all the experiments and it refers to ultrapure deionized water of 180 Ω S cm (Millipore AG, Switzerland).

A. CND synthesis

N-CNDs-1 and **N,S-CNDs** were prepared using a sophisticated microwave Multiwave Pro (Anton Paar, Germany) in HVT50 pressure vessels made of Poly(tetrafluoroethylene) with an additional modifier Perfluoro (propylvinylether) (referred as PTFE-TFM) and **N-CNDs-2** were prepared in a domestic microwave (Imtron GmbH, Germany).

N-CNDs-1: Each vessel was loaded with an aqueous solution consisting of citric acid (1.5 g, 7.8 mmol), ethylenediamine (1.4 g, 23.4 mmol), and MilliQ water (6 ml). Vessels (24) were loaded in the microwave and irradiated at a power of 1200 W [(1) 1 min from 0 to 1200 W, hold 15 min at 1200 W; (2) 1 min from 0 to 1200 W, hold 30 min at 1200 W] (must reach >200 °C).

N,S-CNDs: Each vessel was loaded with an aqueous solution consisting of citric acid (0.75 g, 3.9 mmol), L-cysteine (0.47 g, 3.8 mmol), and MilliQ water (3 ml). Twenty vessels were loaded into the microwave and irradiated at a power of 1200 W (1 min from 0 to 1200 W, hold 13 min at 1200 W). The resulting black syrup was diluted with $NaOH_{aq}$ (1M).

N-CNDs-2: Citric acid (10.50 g, 54.7 mmol, 1 eq.) was dissolved in MilliQ water (38.50 ml) in a 300 ml Erlenmeyer flask and ethylenediamine (75%, 14.00 ml, 164.1 mmol, 3 eq.) was added. The mixture was irradiated at a power of 800 W for 7 min.

Collected fractions were dialyzed against MilliQ water through a dialysis membrane (regenerated cellulose membrane, 1 kDa) for several days until the washing solution remained colorless. CNDs were then lyophilized giving *N*-CNDs-1 (112.3 mg) as a brown powder, *N,S*-CNDs (657.4 mg) as a brown powder, and *N*-CNDs-2 (33.0 mg) as a pale brownish powder.

B. CNDs characterization

Mean hydrodynamic diameter and polydispersity of CNDs in MilliQ water at a concentration of 1 mg/ml were analyzed by Taylor-dispersion analysis (TDA) previously described by Urban *et al.*²² Briefly, sizing experiments were performed using an ActiPix D100 UV-vis area imaging detector (Paraytec, York, UK, 20 Hz sample rate). The detector uses a sensor array, with 1280 columns by 1024 rows, giving a total of 1.3 megapixels. Each pixel has a size of $7 \times 7 \mu\text{m}$, so a total of $49 \mu\text{m}^2$ is imaged. Particle suspensions were injected into a fused silica capillary (Polymicro Technologies, Phoenix, USA) under continuous flow conditions, using a capillary electrophoresis injection system (Prince 560 CE Autosampler, Prince Technologies B.V., Netherlands). The total capillary length ($74.5 \mu\text{m}$ inner diameter) was 130 cm, with the length to the end of the first window being 45 cm and the length to the end of the second window being 85 cm, and a total window length of 1 cm. The detector and capillary were placed inside of the injection system to allow for temperature regulation, which was kept constant at 25 °C.

Infrared spectra were recorded on a Jasco FT/IR-4100 (FTIR, Jasco Europe S.R.L., Italy) spectrometer in the solid state. Elemental analysis was conducted using a Flash2000 Organic Elemental Analyzer (Thermo Scientific, USA), each measurement was performed using 2 mg of CNDs and in duplicate. ζ potentials were recorded using a 90Plus Particle Size Analyzer (Brookhaven, USA) in MilliQ water at a concentration of $20 \mu\text{g}/\text{ml}$. The absorption spectra were recorded on a Jasco V-670 spectrophotometer (Jasco Europe S.R.L., Italy) using 10 mm path length quartz cuvettes. The emission spectra were measured via Cary Eclipse fluorescence spectrometer (Agilent, USA) using 10 mm path length cuvettes at an excitation wavelength of 360 nm. In order to visualize the particle morphology, transmission electron microscope (TEM; Fei Technai Spirit, Oregon, USA) operating at 120 kV was used. CNDs diluted in MilliQ water at a concentration of 1 mg/ml were pipetted onto TEM copper grid. Representative TEM images (supplementary material³⁹) were captured using a Veleta CCD camera (Olympus, Japan).

C. 3D human lung epithelial tissue barrier model

1. Cell cultures

Experiments were carried out using the human alveolar epithelial type II cell line A549, primary MDM and MDDC. The A549 cell line (ATCC CCL-185) was obtained from the American Type Culture Collection (ATCC, USA); cultured in Roswell Park Memorial Institute medium (RPMI 1640) supplemented with 10% (v/v) fetal bovine serum (FBS), 1% (v/v) L-glutamine, and 1% (v/v) penicillin/streptomycin; and

placed in a humidified incubator (37 °C, 5% CO₂). Human blood monocytes (MDM and MDDC) were isolated from buffy coats provided by the blood donation service SRK Bern as previously described by Lehmann *et al.*²³ and purified using CD14 magnetic beads (Microbeads, Milteny Biotech, Germany).²⁴ Monocytes were cultured at a density of 10^6 cells/ml in supplemented RPMI 1640 with the growth factors allowing cells to differentiate [granulocyte-macrophage colony-stimulating factor and interleukin 4 (IL-4) (both 10 ng/ml) for MDDC and M-CSF (10 ng/ml) for MDM] for 7 days. Isolated MDDC and MDM from one donor were used for one independent data set. Whole experiment was repeated four times, using cells from four different donors and four different A549 cell passages.

2. 3D coculture model

The cocultures were prepared as previously described.^{21,25} Transparent BD Falcon cell culture inserts (surface area of 0.9 cm^2 , pores of $3.0 \mu\text{m}$ diameter, polyethylene terephthalate membranes for 12-well plates; BD Biosciences) were placed in BD Falcon tissue culture plates (12-well plates; BD Biosciences) containing 1.5 ml medium (lower chamber), and A549 cells (28×10^4 cells/cm², in 0.5 ml) were seeded in the upper chamber. After 5 days of culturing the A549 cells, the coculture was assembled by adding MDM and MDDC. Briefly, the inserts were placed in a Petri dish turned upside down, and the cells at the bottom of the membrane were gently abraded with a cell scraper. MDDC (69×10^4 cells/cm²) was then pipetted onto the bottom side of the inserts and incubated for 70 min at 37 °C and 5% CO₂. Afterwards, the inserts were placed back into the well plate containing 1.5 ml of pre-heated fresh supplemented RPMI medium. Finally, MDM (1.4×10^4 cells/cm², 0.5 ml) were gently added on the top of the A549 cells and the cocultures were incubated for an additional 24 h. The cells were then exposed to air at the ALI for an additional 24 h prior to exposure by removing the upper medium and replacing the medium from the lower chambers with 0.6 ml of fresh supplemented RPMI.

D. Cell exposure

The cells were washed in the basal compartment with PBS (Gibco, USA) and subsequently transferred to FluoroBrite Dulbecco's modified Eagle's medium (DMEM) Media (DMEM-based formulation with 90% lower background fluorescence signal than the standard phenol red-free DMEM) supplemented with 10% (v/v) FBS, 1% (v/v) L-glutamine, and 1% (v/v) penicillin/streptomycin. The particles were diluted to working concentration with supplemented FluoroBrite DMEM Media, and 100 μl of the suspension was immediately applied on the apical side of the coculture model. The cocultures were previously exposed to air for 24 h, and 100 μl of CNDs suspension was applied on top of the coculture model. As the volume of suspension is rather low, this most likely does not influence the preformed layer of the surfactants. Hereby, mentioned application is referred to as the pseudo-ALI approach (as previously described by Endes

et al.²⁶). The volume of CND suspensions (100 μ l), covering surface of the coculture model, form a thin layer, so the majority of the particles are assumedly to be directly in contact with the cell surface. Therefore, the total CND deposition was assumed to be in the range of $\sim 11 \mu\text{g}/\text{cm}^2$ (100 μ l of 100 $\mu\text{g}/\text{ml}$ suspension applied on the surface area of 0.9 cm^2). The cells were exposed for 1, 4, and 24 h in order to investigate the kinetics of the particle translocation through the cell layer. The applied concentration was carefully chosen based on the detection limit of the spectrofluorometer.

E. Biological response

Samples were collected after 24 h of exposures to CNDs for laser scanning microscopy [LSM; fixed in 4% paraformaldehyde (PFA), see the procedure below], and basal medium was immediately cooled to -80°C after the collection for further cytokine measurements.

1. Cytotoxicity

The release of lactate dehydrogenase (LDH) into the supernatant as a result of cell membrane rupture is a well-known indicator of cytotoxicity. The amount of LDH release was evaluated using a commercially available LDH diagnostic kit (Roche Applied Science, Germany), according to the manufacturer's protocol. Each sample was tested in triplicates, and the enzyme activity was measured photometrically. The absorbance was measured at 490 nm with reference wavelength of 630 nm. Triton-X (0.2% in sterile filtered ultrapure water) applied apically served as a positive control. LDH values are presented relative to the negative control (untreated cells).

2. Cell layer integrity assessment

Effects on the impairment of cell layer integrity after exposure to CNDs were assessed via two complementary approaches by assessing (i) the permeability of cocultures to fluorescein isothiocyanate (FITC)-dextran and (ii) via transepithelial electrical resistance (TEER) technique. All the solutions were prepared freshly prior to the experiments. Hank's Balanced Salt Solution without Ca^{2+} and Mg^{2+} salts (HBSS) was used for the preparation of ethylenediaminetetraacetic acid (EDTA) solution for both assays. The rationale behind the selection of the HBSS (without Ca^{2+} and Mg^{2+} salts) is in the action of the chemical positive control for tight junction disruption, i.e., EDTA, which acts as a divalent cation chelator.

a. Cell resistance measurements. After 24 h exposures to CNDs, cocultures grown on membrane inserts were washed with PBS and TEER measurements (Millicell[®] ERS-2, EMD Millipore Corporation, MA, USA) were performed on three defined spots on each membrane insert (1.5 ml of PBS in the lower and 0.5 ml of PBS in the upper compartments). Resistance values of two empty (without cells) membrane inserts were averaged (after two independent sets of measurements) and subtracted from all the values measured in the presence of the cells. The absolute values were multiplied by the growth area of membrane inserts (0.9 cm^2) and shown in

$\Omega\text{-cm}^2$. Positive control samples were treated with EDTA (2.5 mM in HBSS, 60 min).

b. Assessment of cell layer permeability to FITC-dextran (70 kDa). A stock solution of EDTA (0.5M in MilliQ water) was diluted in HBSS to 5 mM. A fluorescein isothiocyanate-dextran solution [70 kDa; FITC-dextran (25 mg/ml) in MilliQ water] was diluted to 4 mg/ml (2 \times concentrated) in HBSS. After TEER measurements, cocultures were washed with HBSS and subsequently placed in 12-well cell culture plates containing 600 μ l HBSS in the lower chamber. Then, 250 μ l of HBSS was added in the upper chambers of untreated and CND-exposed cocultures as well as two empty inserts; 250 μ l of 5 mM EDTA (=2 \times concentrated, will be further diluted with FITC-dextran solution) in HBSS was used as the positive control samples. Solution of 250 μ l of the FITC-dextran solutions (4 mg/ml) in HBSS was added in the upper chambers of all the samples and incubated for 60 min (dark, 37°C). After incubation, membrane inserts were immediately removed from the cell culture plates; the supernatants of HBSS containing FITC-dextran were collected from the lower chambers (precise volumes were noted for each sample individually) and kept in dark until the measurements. The fluorescence measurements were subsequently conducted in triplicates in black 96-well plates using the microplate reader (Tristar LB 941, Berthold Technologies; using the following filters setup: $\lambda_{\text{ex}}/\lambda_{\text{em}}$: 485/535 nm). Results were expressed as % of permeability to FITC-dextran normalized to the supernatant volumes and relative to the average values of the empty (blank) inserts.

3. Oxidative stress

The intracellular reduced glutathione (GSH) content of the cocultures was determined using the Glutathione Assay Kit (Cayman Chemical, MI, USA) according to the manufacturer's protocol. After 24 h exposures to CNDs, cocultures cultivated on the membrane inserts were washed with PBS and cells were detached from the membranes via cell scarper (600 and 100 μ l of cold 2-(N-morpholino)ethanesulfonic acid buffer in the upper and lower chambers, respectively). Total protein amount of each sample was quantified via Pierce BCA Protein Assay Kit, Thermo Fisher Scientific Inc., USA. The results are presented as the total intracellular GSH content (in μM) relative to the total protein content. Cocultures exposed apically to 100 μ l of L-buthionine-sulfoximine [BSO; Sigma-Aldrich GmbH, Buchs, Switzerland; (200 μM) in supplemented FluoBrite DMEM] for 24 h were used as a positive control.

4. Cytokine quantification

The (pro-)inflammatory response of the cocultures after CNDs exposure was measured by quantifying the amount of tumor necrosis factor α (TNF- α) and interleukin 1 β (IL-1 β) and interleukin 8 (IL-8) (pro-)inflammatory mediators released into the lower medium chamber via enzyme-linked immunosorbent assay (ELISA) using the commercially available DuoSet ELISA Development Kit (R&D Systems, Switzerland) according to the supplier's protocol. Cocultures treated with lipopolysaccharide

[LPS from *Escherichia coli* at 1 µg/ml] for 24 h acted as the positive control for the (pro-)inflammatory response.

5. Laser scanning microscopy

The cocultures were fixed for 15 min in 4% PFA in PBS after the 24 h exposure. To investigate cell morphology, fixed samples were stained with 4',6-diamidino-2-phenylindole dihydrochloride (2 µg/ml; Sigma-Aldrich, Switzerland) and phalloidin rhodamine (0.132 µM; Invitrogen, USA) for 1 h and subsequently embedded in Glycergel. An inverted laser scanning confocal microscope (LSM 710, Zeiss, Germany) was used for the sample visualization. Image processing was performed using the restoration software IMARIS (Bitplane AG, Switzerland).

F. Particle distribution

1. Sample collection

After the exposure (i.e., 1, 4, or 24 h), the samples were collected for further investigation. For spectrofluorometric analysis, samples were collected as follows: The basal medium was first collected; then, the top of the cells was washed with 1 ml of PBS and subsequently collected as apical wash. Finally, 1 ml of PBS was applied on the top of the coculture model, and cells (from both sides of membrane) were scraped using a cell scraper and collected. All the collected samples were investigated within 1 h after the collection.

2. Spectrofluorimetry

The apical wash, scraped cells, and basal medium were measured via plate reader (Tristar LB 941, Berthold Technologies) using the following filters setup: $\lambda_{\text{ex}}/\lambda_{\text{em}}$: 355/470 nm. The amount of CNDs in each fraction was calculated based on the standard curve equation (separate curves for each CND sample, condition, and time-point) using the reading values. Freshly diluted CNDs in corresponding media (i.e., supplemented FluoroBrite DMEM or PBS) served as standards; the known concentrations applied were carefully chosen to be within the linear range of the reading, subsequently the linear curve was plotted to obtain the standard curve equation for further calculations.

G. Statistical analysis

All data are presented as mean \pm standard error of the mean. A total of four independent experiments ($n = 4$) were performed for the fractional measurements of the CNDs, cell viability, oxidative stress, and (pro-)inflammatory cell responses. Statistical analysis was performed using GRAPHPAD PRISM (GraphPad Software Inc., La Jolla, USA). Assuming normal distribution of the data sets, a parametric one-way analysis of variance (ANOVA) was performed, followed by Dunnett's multiple comparison test. Results were considered significant if $p < 0.05$.

III. RESULTS

A. Particle synthesis and characterization

Citric acid was used as carbon source for the synthesis of the CNDs, and the particles were doped with nitrogen using ethylenediamine to form *N*-CNDs or codoped with nitrogen

and sulfur using cysteine to form *N,S*-CNDs [Fig. 1(a)]. Precursors were carbonized by microwave irradiation using a sophisticated microwave (*N,S*-CNDs and *N*-CNDs-1) or a domestic microwave (*N*-CNDs-2) with optimized parameters. The transparent starting solutions resulted in brown-colored solutions upon the formation of CNDs which were dialyzed against MilliQ water. After lyophilization, CND stock solutions were prepared in MilliQ water at a concentration of 10 mg/ml, and after several days, *N*-CNDs-1 revealed strong agglomeration, while *N,S*-CNDs showed a tendency to agglomerate, and *N*-CNDs-2 displayed better dispersability [Fig. 1(b)].

The CNDs were characterized by various methods to determine their physicochemical properties including TDA, ζ potential (Table I; FTIR, Fig. 2), and elemental analysis.

TDA was the method of choice to determine the size of the prepared CNDs as it is appropriate for calculating the size of nanoparticles or small molecules, which are often difficult to describe using conventional methods such as dynamic light scattering or transmission electron microscopy.²² Our TDA data showed that *N,S*-CNDs and *N*-CNDs-2 were very small particles, having hydrodynamic diameters of 0.9 and 1.4 nm, respectively (Table I). These sizes are the smallest reported for CNDs in the literature; however, to our knowledge, this study marks the first time that the size of CNDs size has been determined by TDA. The size of *N*-CNDs-1 could not be determined because of strong agglomeration which resulted in blocking of the measurement tubes. Representative TEM images of *N*-CNDs-1 showed the agglomeration of the sample [supplementary material, Fig. S1 (Ref. 39)].

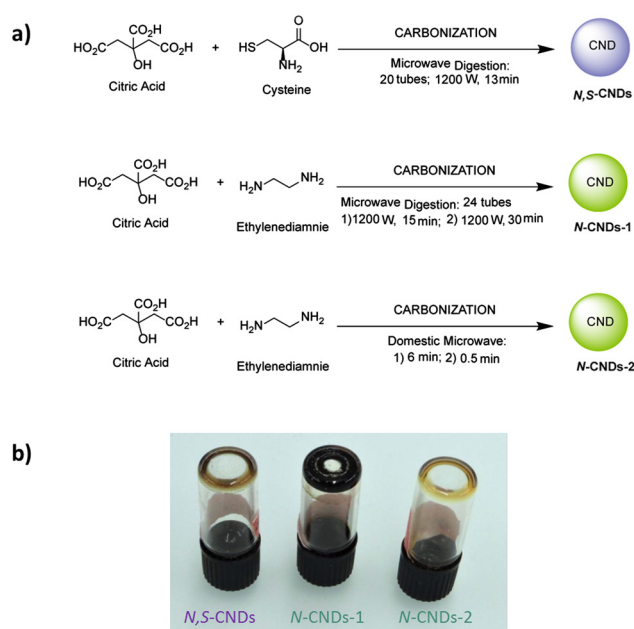


FIG. 1. (a) Synthesis of CNDs. (b) Dispersion behavior and agglomeration state of CNDs stock solution in MilliQ water (10 mg/ml) after several days; the vial has been turned upside down: *N,S*-CNDs showed minor agglomeration, *N*-CNDs-1 showed strong agglomeration, *N*-CNDs-2 formed in stable dispersions.

TABLE I. Physicochemical properties of CNDs: hydrodynamic diameter obtained by TDA and ζ potential.

CNDs type	Hydrodynamic diameter by TDA (nm)	ζ potential (mV)
<i>N,S</i> -CNDs	0.90	-15.7
<i>N</i> -CNDs-1	—	+14.9
<i>N</i> -CNDs-2	1.42	+3.5

As observed in the FTIR spectra (Fig. 2), all CNDs present bands in the region between 3000 and 3500 cm^{-1} corresponding to the stretching vibrations of the OH and NH_2 groups. The characteristic bands corresponding to the amide bonds, resulting from the condensation between carboxylic acid and amine groups, were also present in the three different CNDs with the stretching vibrations of C=O at 1640 cm^{-1} , N-H at 1555 cm^{-1} , and C-N at 1440 cm^{-1} , respectively. In addition, *N,S*-CNDs also showed bands corresponding to carboxylic groups, namely, the C=O (1698 cm^{-1}) and C-O (1215 cm^{-1}) stretching vibrations. Thiol group was also presented with a broad band at 2550 cm^{-1} .

The overall charge of CNDs measured by ζ potential measurement showed that *N*-CNDs-1 were positively charged, which is likely due to the presence of a high density of amine groups on the surface; *N*-CNDs-2 were found to be neutral, which can be attributed to the formation of amide groups as confirmed by the high intensity of the bands at 1640 and 1555 cm^{-1} in the infrared spectrum (Fig. 2), presumably a result of the longer reaction time.²⁷ In contrast,

N,S-CNDs were negatively charged, confirming the presence of carboxylic groups on the surface, which we attribute to the use of cysteine as synthetic precursor.

Furthermore, the chemical composition of CNDs measured by elemental analysis showed the successful doping of CNDs with nitrogen in *N*-CNDs and nitrogen and sulfur in *N,S*-CNDs [supplementary material, Table SI (Ref. 39)]. Interestingly, *N*-CNDs-2, which are stable in suspension, showed higher hydrogen content (7% for *N*-CNDs-2 versus 4% for *N*-CNDs-1 and *N,S*-CNDs), while the less colloidal stable *N*-CNDs-1 had higher carbon content, which can be attributed to the presence of a greater proportion of amorphous carbon features (fewer functional groups on the surface).²⁸

The photophysical measurements showed that CNDs possess a strong absorption in the UV region with a tail in the visible region which is a typical feature of CNDs.²⁹ However, the UV-vis absorption curves were found to differ for each type of CNDs, an effect that was attributed to different surface structures [Fig. 3(a)]. Specifically, the samples had an absorption at 240 nm, corresponding to $\pi \rightarrow \pi^*$ transitions of the aromatic sp^2 domains, and a band at 335–375 nm assigned to the $n \rightarrow \pi^*$ transition of the surface groups. The latter absorption band in the spectrum of *N*-CNDs-2, centered at 345 nm, is strong and symmetrical in contrast to those of the *N,S*-CNDs and *N*-CNDs-1 samples, which form weak shoulder bands at 335 and 375 nm, respectively. This is in agreement with previous structural observations in which *N*-CNDs-2 were suggested to contain more amide and carbonyl groups on their surface.³⁰ In addition, the low

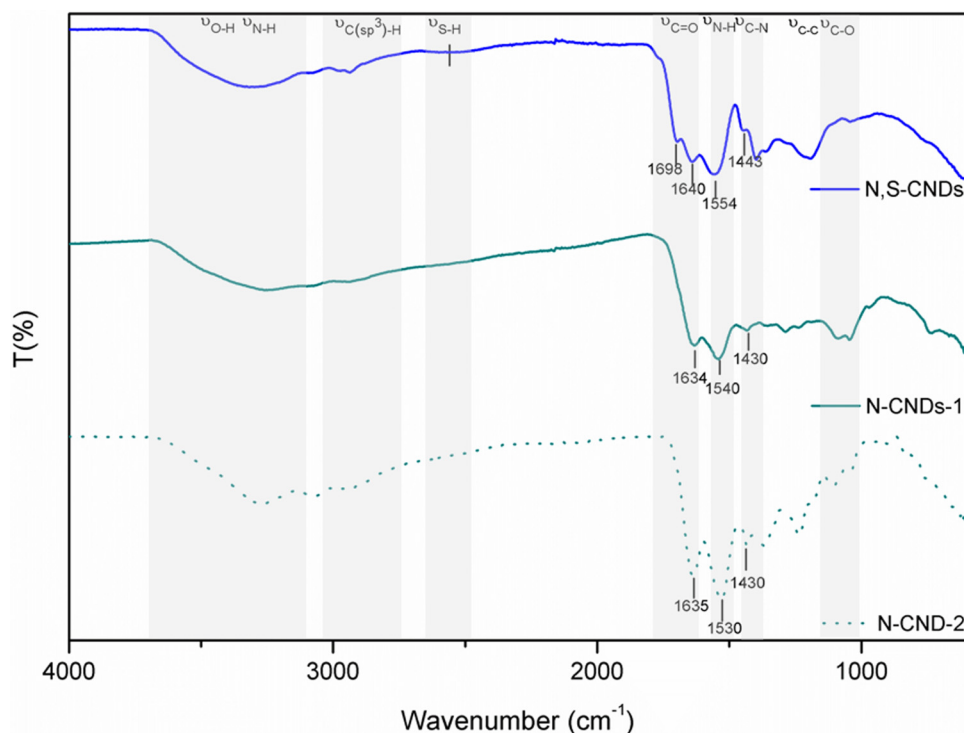


FIG. 2. FTIR spectra of all three types of CNDs.

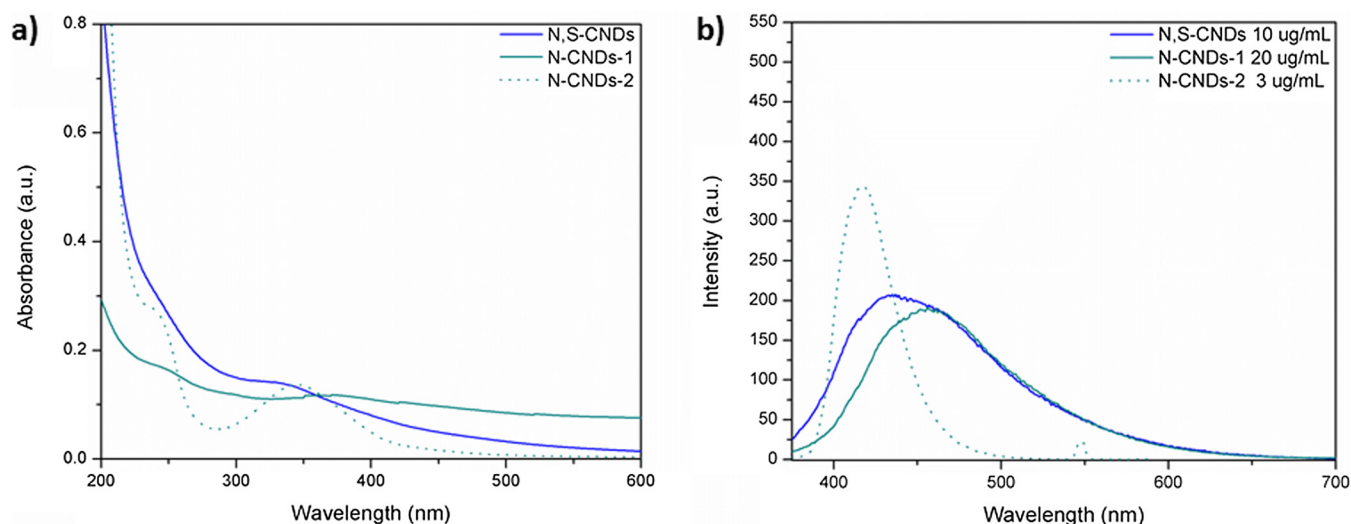


Fig. 3. (a) UV-vis absorption spectra of CNDs (20 µg/ml in MilliQ water). (b) Fluorescence spectra of CNDs in MilliQ water at an excitation wavelength of 360 nm.

absorption of *N-CNDs-1* in the lower UV region also confirms its higher proportion of amorphous carbon.

The fluorescence of the CNDs was measured at the excitation wavelength of 360 nm. The emission appeared to be much stronger and sharper for *N-CNDs-2*, indicating a higher photoluminescence quantum yield (i.e., ca. 6 and 12 times the intensity of *N,S-CNDs* and *N-CNDs-1*, respectively) [Fig. 3(b)]. The peak emission intensity was centered at 417, 432, and 455 nm for *N-CNDs-2*, *N,S-CNDs*, and *N-CNDs-1*, respectively. The UV-vis and fluorescence spectra of all three types of CNDs in supplemented FluoroBrite DMEM are shown in Fig. S2 of the supplementary material,³⁹ showing no change in either their absorption or fluorescence properties over 24 h. These findings demonstrate that the CNDs synthesized herein do not modify their colloidal stability in cell culture media, making them good candidates for further study in the lung model.

B. Exposure of CNDs to the lung model

CNDs were then exposed to the lung coculture model under pseudo-ALI conditions as previously described by Tomašek et al.³¹ for the application of hydrophobic materials such as diesel particles. After 24 h exposures to CNDs, cell viability, assessed via quantification of LDH (intracellular enzyme released into the medium when cell membrane is ruptured), showed no increase compared to untreated cells [Fig. 4(a)], whereas for the positive control (Triton-X) a significant ($p < 0.05$) increase could be shown. A minor decrease (thus not statistically significant) of cell layer permeability for the *N,S-CNDs* treated cocultures was observed, while *N-CNDs* did not influence the cell layer permeability compared to the untreated cells [Fig. 4(b)]. There was no decrease in TEER values observed for all the three types of CNDs [Fig. 4(c)]. Furthermore, based on the LSM data, we have concluded that there was no difference in cell morphology of CND-treated cells in comparison to untreated samples [Fig. 4(d)]. In

addition, exposures to CNDs induced no statistically significant depletion of the total intracellular GSH levels [Fig. 5(a)] in the cocultures as well as there was no increase in the release of the tested (pro-)inflammatory markers [TNF- α , IL-1 β , and IL-8; Figs. 5(b)–5(d)].

As no adverse effect of CNDs toward the 3D human lung model was observed, a thorough investigation of the particle translocation kinetics was performed in order to better understand the possible CNDs behavior in human body. The fractional distribution of CNDs in three different compartments was evaluated after their exposure to the lung cocultures. CNDs can potentially remain on the cell surface (apical side), be internalized by or associated with macrophages and epithelial cells, or translocated across the cellular barrier into the basolateral side, as depicted in Fig. 6(a). The CND concentration was determined in each fraction (i.e., apical, intracellular, and basal) by measuring the corresponding fluorescence intensity via plate reader after 1, 4, and 24 h of exposure. It was observed that the fraction of CNDs on the apical side generally decreases over time [Fig. 6(b)]. Only 40% of *N-CNDs-2* remained apical after 1 h, while more than 80% remained on the apical side with *N,S-CNDs* and *N-CNDs-1*. Conversely, an increase over time was seen in the basal fraction for *N-CNDs*, while *N,S-CNDs* were below the detection limit [Fig. 6(c)]. Almost 100% of *N-CNDs-2* were translocated after only 4 h, while *N-CNDs-1* showed only 20% of translocation after 4 h which did not increase further. Quantification of CNDs in the intracellular fraction proved to be more challenging, especially for *N,S-CNDs* and *N-CNDs-1*, which possess weak fluorescence properties [Fig. 6(d)]. However, a significant amount of *N-CNDs-1* (45%) was measured in the intracellular fraction 24 h postexposure. In contrast, only a small amount of *N-CNDs-2* was detected intracellularly after 1 h, which remained constant until the 24 h mark.

Figure 6(e) shows the cumulative amount of CNDs estimated from the sum of the fluorescence intensity in the apical, intracellular, and basal fractions after 1, 4, and 24 h of

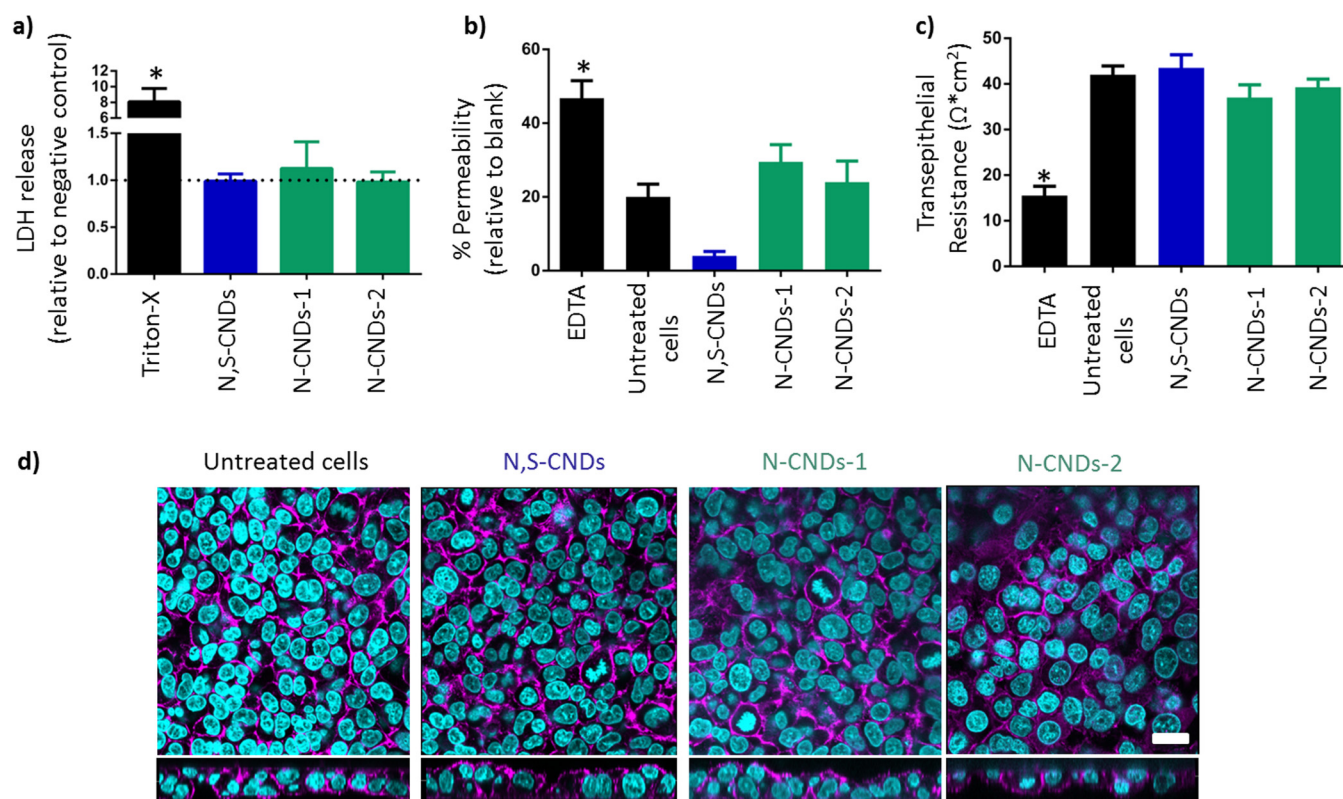


FIG. 4. Effect of CNDs on cell viability, integrity, and morphology of the 3D lung model after 24 h exposures to CNDs. (a) Cell viability assessed by the release of the intracellular enzyme LDH 24 h after exposure to CNDs. Triton-X (0.2% in MilliQ water, 24 h) was applied as a positive control. Cell layer integrity evaluated via (b) permeability to Dextran-FITC (70 kDa) and (c) TEER levels. EDTA (2.5 mM in HBSS) was applied as a positive control. Data are presented as mean \pm standard error of the mean ($n=4$). Data marked as (*) were considered to be increased by a statistically significant amount compared to negative control (untreated cells) ($p < 0.05$). (d) LSM images of cocultures exposed to CNDs at xy projection (upper) and xz projection (lower) presenting the coculture setup. Magenta shows the F-actin cytoskeleton and cyan the nuclei. Scale bar: 20 μm .

exposition time, presented as stacked columns and expressed as a percentage of the deposited mass. *N,S-CNDs* and *N-CNDs-1* show a decrease over time from 100% after 1 h to less than 50% after 4 h. A possible explanation for this is that *N,S-CNDs* and *N-CNDs-1* are unstable when coming into contact with cells, and that agglomeration can induce measurement artifacts. It is important to note that internalized CNDs could not be reliably measured as the autofluorescence signal of the cells was significantly higher than the fluorescence signal of the CNDs. On the other hand, *N-CNDs-2* which are stable and possessed a stronger fluorescent signal show a constant recovery of 100% over 24 h.

Consequently, the distribution of *N-CNDs-2* can be measured with good precision over 24 h. As for *N,S-CNDs* and *N-CNDs-1*, measurements remain valid up to 1 h, but subsequently become unprecise; however, a tendency can still be observed.

IV. DISCUSSION

Understanding the deposition, interaction, and translocation of ultrafine particles below 5 nm remains challenging because of analytical limitations due to their small size. The unique properties of CNDs, namely, their fluorescence properties, their small size (<10 nm), and their similarity in structure to the airborne

ultrafine carbon particles, make them ideal candidates to gain a better understanding of the mechanistic interactions of particles at the lung barrier. Hence, CNDs of different compositions were prepared to investigate the effects of surface properties on the cell response and/or translocation across the lung barrier model. In total, three different types of CNDs with different surface characteristics were prepared and their cellular association in the 3D lung model was investigated. Characterization of the CNDs confirmed their successful formation and doping with nitrogen and nitrogen/sulfur. Positively charged *N-CNDs-1*, bearing amide groups at the surface, displayed a highly amorphous profile, which could explain the strong agglomeration observed in both supplemented FluoroBrite DMEM and MilliQ water, as well as their poor fluorescence properties (i.e., low photoluminescence). In contrast, neutral *N-CNDs-2*, with a hydrodynamic diameter of 1.4 nm, exhibited a surface containing organic groups such as amide, amino, and hydroxyl groups, possessed very stable dispersions in MilliQ water, and were found to have intense fluorescence. Negatively charged *N,S-CNDs* decorated with additional carboxylic and thiol groups, with a hydrodynamic diameter of 0.9 nm, exhibited fewer organic groups on the surface than *N-CNDs-2*, but at the same time were not as amorphous as *N-CNDs-1*, which resulted in a tendency to agglomerate in MilliQ water and weak-to-moderate fluorescent signals.

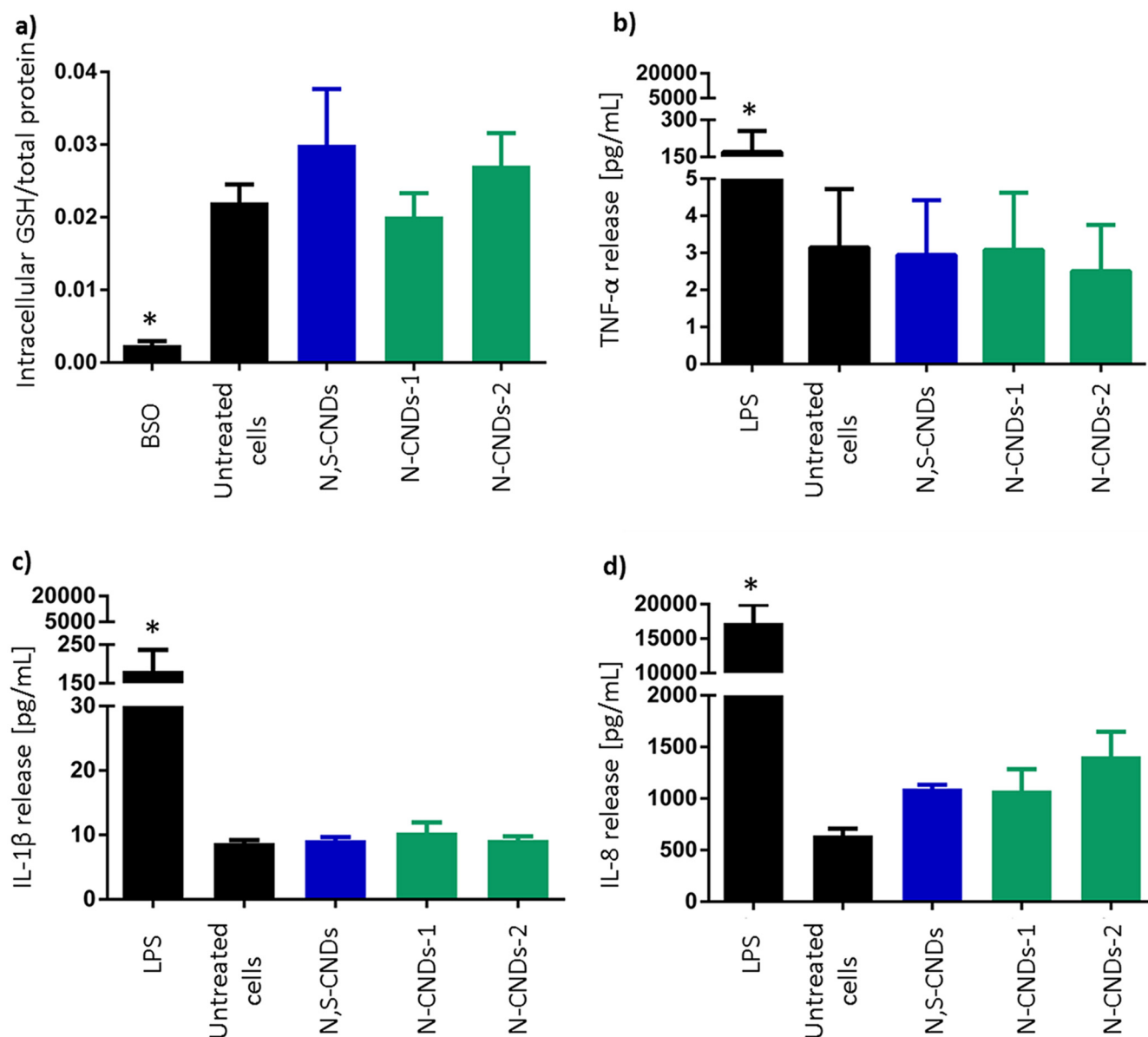


Fig. 5. Biochemical response, i.e., oxidative stress levels and (pro-)inflammatory response, of the 3D lung model after 24 h exposures to CNDs. (a) The total intracellular GSH content normalized per total protein content. BSO (200 μ M in supplemented FluoroBrite DMEM, 24 h) was used as a positive control of intracellular GSH depletion. [(b)–(d)] Release of (pro-)inflammatory cytokines TNF- α (b), IL-1 β (c), and IL-8 (d). LPS (1 μ g/ml in supplemented FluoroBrite DMEM) was used as a positive control for the secretion of (pro-)inflammatory markers. Data are presented as mean \pm standard error of the mean ($n = 4$). Data marked as (*) were considered statistically significantly increased compared to negative control (untreated cells) ($p < 0.05$).

As hereby mentioned, CNDs are meant to be the model system simulating carbonaceous material in the environment; therefore, the realistic exposure doses can be estimated as follows: A healthy, moderately active adult could assumedly reach a daily inhaled air volume of 25 m³ with an alveolar lung surface area of about 100 m² and an alveolar deposition efficiency of about 10–50% (for 10–100 nm particles).³² The realistic daily average dose level, therefore, is estimated in an urban environment to be 7.5×10^{-5} mg/cm² (particle mass per cm² lung epithelium; 24 h clearance from the alveolar region is negligible), assuming an ultrafine particle mass concentration of 10 mg/m³ (particles with mobility diameter <100 nm).³²

We have chosen a relatively high, but based on the results above still nontoxic, concentration of 100 μ g/ml of CNDs under pseudo-ALI conditions, corresponding to an estimated total deposition of $\sim 11 \mu$ g/cm². This is about 150-times higher than the daily average dose level for UFPs in urban air and 20 000-times higher than the level of carbon black reported in Switzerland.³³ However, because of the small size of the CNDs and the detection limits of the instruments used for fluorescence measurements, we could not apply a lower concentration.

Biological response of the 3D human lung coculture model to CNDs was assessed after 24 h exposures to three types of CNDs. None of the CND types affected viability [cell membrane integrity assessed via LDH release, oxidative stress status

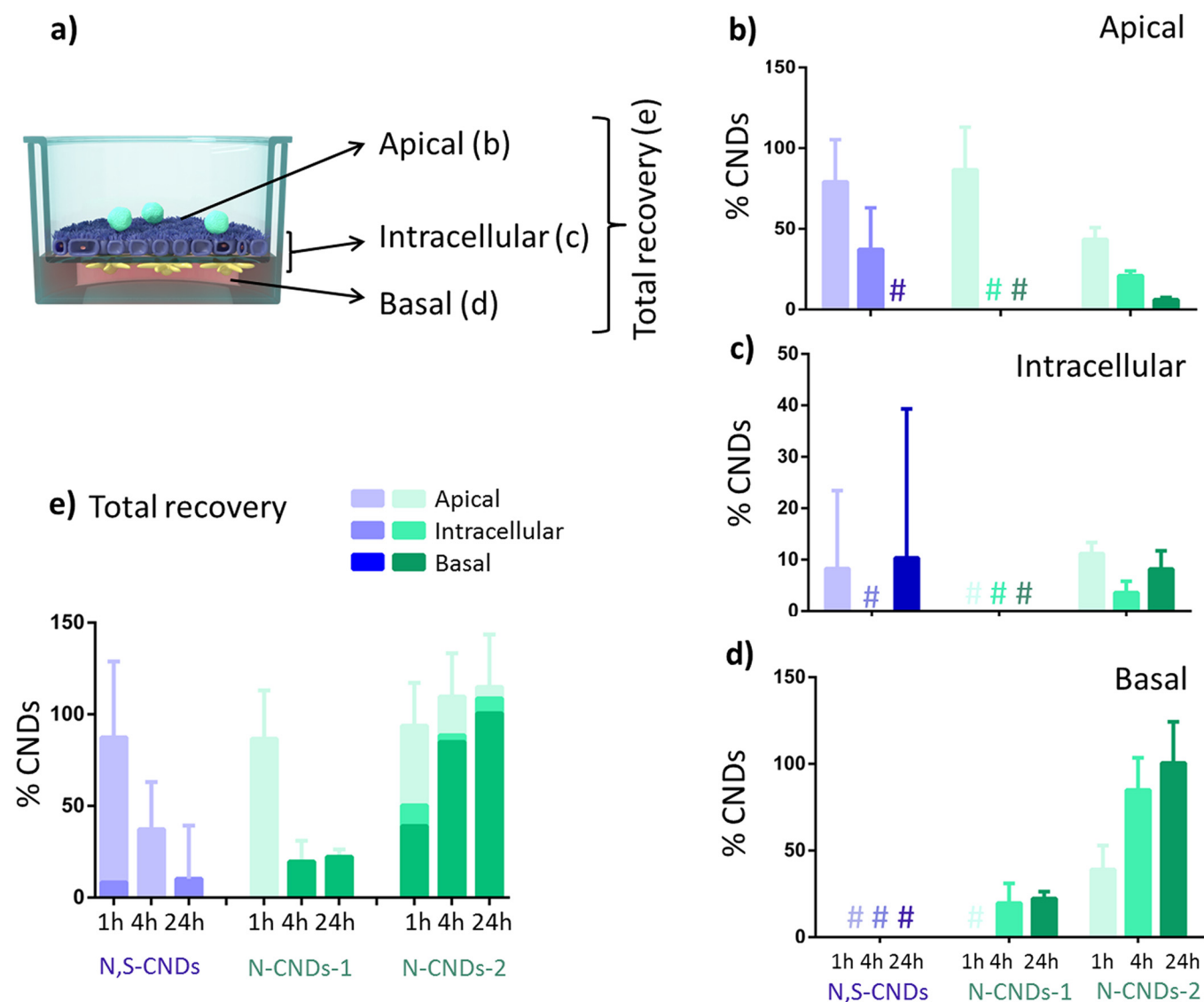


FIG. 6. Biodistribution of the CNDs at the lung model barrier. (a) Scheme of the lung coculture with the different fractions highlighted: apical, intracellular, and basal. Amount of CNDs (%) after exposure in (b) the apical fraction, (c) the basal fraction, and (d) the intracellular fraction. (e) Total cumulative amount of CNDs presenting the total recovery of CNDs after each time-point distinguishing each fraction [apical (light color), basal (middle color), and intracellular (dark color)]. Data are presented as mean \pm standard error of the mean ($n = 4$). Data marked as (#) were below the detection limit of the instrument.

via intracellular GSH levels, (pro-)inflammatory cytokine release (TNF- α , IL-1 β and IL-8)] and cell layer integrity under the tested conditions (100 μ l of 100 μ g/ml at pseudo-ALI). The statistically significant effect (one-way ANOVA, followed by Dunnett's multiple comparison test; $p < 0.05$) was observed for all the tested positive controls (Triton-X, BSO, LPS, and EDTA) and corresponding biological endpoints proving the responsiveness of the employed 3D human lung model.

Fluorescence measurements of CNDs can be used to investigate the cellular uptake,³⁴ and in the current study, the fractions of CNDs were assessed in the different compartments of the 3D lung model. The reliability of the measurements was assessed by measuring the correlation between the applied amount of CNDs and the measured amount of CNDs after exposure time. A good recovery rate was observed with N-CNDs-2 (i.e., $\sim 94 \pm 23\%$, $109 \pm 24\%$, and $114 \pm 29\%$ after

1, 4, and 24 h, respectively). Similar values were also obtained for N,S-CNDs (79%) and N-CNDs-1 (87%) after 1 h of exposure; however, for longer exposure times, the recovery rate was significantly below 100%, since the fluorescence measurements were at the limit of the detection and thus these values were not considered for the discussion.

The major fraction of N-CNDs-2 ($\sim 85\%$) was found to be translocated after 4 h, while a small amount was detected in the apical wash ($\sim 21\%$) and intracellularly ($\sim 4\%$). Previous studies with different particles have shown a major fraction to be retained in the lung and a minor fraction translocated, both *in vitro* ($< 5\%$)^{25,35} and *in vivo* ($< 2\%$).^{36,37} However, most of these particles are metal-based (i.e., gold) and have higher hydrodynamic diameters (between 5 and 200 nm). Kreyling *et al.*³⁷ instilled mice with gold nanoparticles of various sizes and showed that with negatively charged 1.4 nm gold

nanoparticles, the translocation across the lung tissue was continuous until 3 h after exposure in the range of 5%. However, the authors did not determine if the particles were agglomerated or not. In the present study, the particles are significantly different, as the CNDs are composed of a carbon core with an organic surface and have very small hydrodynamic diameters (<2 nm). Interestingly, particles similar to the CNDs used in the current study also showed high translocation *in vivo*.³⁸ Carbon nanoparticles, such as organic and hybrid (inorganic/organic) nanoparticles with hydrodynamic diameters of 5 and 7 nm, respectively, were found to be ~50% translocated 1 h after deposition in the rat lung. The translocation of *N*-CNDs-2 was found to be 40% after only 1 h, while ~44% remained on the apical surface, which means only a minor fraction (~12%) was intracellular. Due to their low cellular uptake, together with difficulties associated with visualizing the CNDs alone (low fluorescence signals with emission spectra overlapping with the background and cell emission spectra) by LSM [see supplementary material, Fig. S3 (Ref. 39)], it is thus not possible to postulate a para- or transcellular translocation pathway.

Comparison of the translocated CNDs after 1 h showed that 40% of the *N*-CNDs-2 particles were found in the basal side, whereas *N*-CNDs-1 and *N,S*-CNDs mostly remained (~80%) on the apical side. While in a previous study a similar translocation rate was observed for single and aggregated gold nanoparticles using the same *in vitro* human 3D cell culture lung model,²⁵ in the present study, the agglomeration significantly affected the translocation of CNDs to the basal side.

V. CONCLUSION

Three types of CNDs with different surface properties were synthesized and thoroughly characterized, including their size, surface properties, and agglomeration behavior. Their biodistribution at the human lung epithelial tissue barrier was then studied at different time points. None of the CNDs caused adverse effects in a human lung epithelial tissue barrier model, and the biokinetics data showed that the translocation behavior strongly depends on the particle properties (surface properties and agglomeration state). However, the small size and weak fluorescence of *N*-CNDs-1 and *N,S*-CNDs made it difficult to obtain reliable biodistribution data for 4 and 24 h. Further research is required to determine the applicability of CNDs as surrogates for carbon-based particles in order to study their mechanistic interactions with biological systems.

ACKNOWLEDGMENTS

This study was supported by the Toyota Motor Corporation and the Adolphe Merkle Foundation.

¹A. L. Braga, A. Zanobetti, and J. Schwartz, *Eur. Respir. J.* **16**, 723 (2000).

²S. A. Bremner, H. R. Anderson, R. W. Atkinson, A. J. McMichael, D. P. Strachan, J. M. Bland, and J. S. Bower, *Occup. Environ. Med.* **56**, 237 (1999).

³D. W. Dockery, C. A. Pope, X. Xu, J. D. Spengler, J. H. Ware, M. E. Fay, B. G. Ferris, Jr., and F. E. Speizer, *N. Engl. J. Med.* **329**, 1753 (1993).

⁴C. A. Pope III, R. T. Burnett, M. J. Thun, E. E. Calle, D. Krewski, K. Ito, and G. D. Thurston, *J. Am. Med. Assoc.* **287**, 1132 (2002).

⁵A. H. Choudhury, M. Gordian, and S. S. Morris, *Arch. Environ. Health* **52**, 113 (1997).

⁶D. E. Abbey, N. Nishino, W. F. McDonnell, R. J. Burchette, S. F. Knutsen, W. Lawrence Beeson, and J. X. Yang, *Am. J. Respir. Crit. Care Med.* **159**, 373 (1999).

⁷E. Aga et al., *Eur. Respir. J.* **21**, 28s (2003).

⁸R. Kaiser, I. Romieu, S. Medina, J. Schwartz, M. Krzyzanowski, and N. Künzli, *Environ. Health* **3** (2004).

⁹A. Zanobetti et al., *Environ. Health Perspect.* **111**, 1188 (2003).

¹⁰A. Nemmar, P. Hoet, B. Vanquickenborne, D. Dinsdale, M. Thomeer, M. F. Hoylaerts, H. Vanbilloen, L. Mortelmans, and B. Nemery, *Circulation* **105**, 411 (2002).

¹¹N. L. Mills et al., *Am. J. Respir. Crit. Care Med.* **173**, 426 (2006).

¹²P. Wiebert, A. Sanchez-Crespo, R. Falk, K. Philipson, A. Lundin, S. Larsson, W. Moller, W. G. Kreyling, and M. Svartengren, *Inhal. Toxicol.* **18**, 741 (2006).

¹³N. Li, S. Georas, N. Alexis, P. Fritz, T. Xia, M. A. Williams, E. Horner, and A. Nel, *J. Allergy Clin. Immun.* **138**, 386 (2016).

¹⁴G. Oberdorster, *Int. Arch. Occup. Environ. Health* **74**, 1 (2000).

¹⁵J. Heyder, J. Gebhart, G. Rudolf, C. F. Schiller, and W. Stahlhofen, *J. Aerosol Sci.* **17**, 811 (1986).

¹⁶J. S. Patton and P. R. Byron, *Nat. Rev. Drug Discov.* **6**, 67 (2007).

¹⁷F. Shirmohammadi, S. Hasheminassab, A. Saffari, J. J. Schauer, R. J. Delfino, and C. Sioutas, *Sci. Total Environ.* **541**, 1083 (2016).

¹⁸J. Wang, G. Liu, K. C.-F. Leung, R. Loffroy, P.-X. Lu, and Y. X. J. Wang, *Curr. Pharm. Des.* **21**, 5401 (2015).

¹⁹Y. Park, J. Yoo, B. Lim, W. Kwon, and S. W. Rhee, *J. Mater. Chem. A* **4**, 11582 (2016).

²⁰P. Miao, K. Han, Y. Tang, B. Wang, T. Lin, and W. Cheng, *Nanoscale* **7**, 1586 (2015).

²¹B. M. Rothen-Rutishauser, S. G. Kiama, and P. Gehr, *Am. J. Respir. Cell Mol. Biol.* **32**, 281 (2005).

²²D. A. Urban, A. M. Milosevic, D. Bossert, F. Crippa, T. L. Moore, C. Geers, S. Balog, B. Rothen-Rutishauser, and A. Petri-Fink, *Colloid Interface Sci. Commun.* **22**, 29 (2018).

²³A. Lehmann, C. Brandenberger, F. Blank, P. Gehr, and B. Rothen-Rutishauser, "A 3D model of the human epithelial airway barrier," in *Alternatives to Animal Testing*, edited by M. L. Yarmush and R. S. Langer (Artech House, Norwood, 2010), pp. 239–260.

²⁴S. Steiner et al., *Atmos. Environ.* **81**, 380 (2013).

²⁵E. Durantie, D. Vanhecke, L. Rodriguez-Lorenzo, F. Delhaes, S. Balog, D. Septiadi, J. Bourquin, A. Petri-Fink, and B. Rothen-Rutishauser, *Part. Fibre Toxicol.* **14**, 49 (2017).

²⁶C. Endes et al., *Part. Fibre Toxicol.* **11**, 1 (2014).

²⁷D. Qu, M. Zheng, L. Zhang, H. Zhao, Z. Xie, X. Jing, R. E. Haddad, H. Fan, and Z. Sun, *Sci. Rep.* **4**, 5294 (2014).

²⁸N. Papaioannou, A. Marinovic, N. Yoshizawa, A. E. Goode, M. E. Fay, A. Khloubystov, M.-M. Titirici, and A. Sapelkin, *Sci. Rep.* **8**, 6559 (2018).

²⁹N. Baker Sheila and A. Baker Gary, *Angew. Chem. Int. Ed.* **49**, 6726 (2010).

³⁰P. Lv, Y. Yao, H. Zhou, J. Zhang, Z. Pang, K. Ao, Y. Cai, and Q. Wei, *Nanotechnology* **28**, 165502 (2017).

³¹I. Tomašek, C. J. Horwell, D. E. Damby, H. Barošová, C. Geers, A. Petri-Fink, B. Rothen-Rutishauser, and M. J. D. Clift, *Part. Fibre Toxicol.* **13**, 67 (2016).

³²ICRP, "Human respiratory tract model for radiological protection," in *Annals of International Commission on Radiological Protection* (Ann ICRP, UK, 1994).

³³H. Olstrup, C. Johansson, and B. Forsberg, *Int. J. Environ. Res. Public Health* **13**, 249 (2016).

³⁴L. Thoo, M. Z. Fahmi, I. N. Zulkpli, N. Keasberry, and A. Idris, *Cent. Eur. J. Immunol.* **42**, 324 (2017).

³⁵G. Bachler, S. Losert, Y. Umehara, N. Von Goetz, L. Rodriguez-Lorenzo, A. Petri-Fink, B. Rothen-Rutishauser, and K. Hungerbuehler, *Part. Fibre Toxicol.* **12**, 18 (2015).

³⁶S. K. Balasubramanian, K.-W. Poh, C.-N. Ong, W. G. Kreyling, W.-Y. Ong, and L. E. Yu, *Biomaterials* **34**, 5439 (2013).

³⁷W. G. Kreyling et al., *ACS Nano* **8**, 222 (2014).

³⁸H. S. Choi et al., *Nat. Biotechnol.* **28**, 1300 (2010).

³⁹See supplementary material at <https://doi.org/10.1116/1.5043373> for elemental analysis of CNDs, TEM micrographs of *N*-CNDs-1, CNDs stability in DMEM, and LSM spectra of CNDs.



Estelle Durantie studied Chemistry at the Ecole Nationale Supérieure de Chimie de Montpellier in France. After her M.Sc., she worked for 1 year at Novartis in Basel, Switzerland, in the development of process synthesis. She then did her Ph.D. at the Swiss Federal

Institute of Technology in Zurich (ETHZ) in the drug delivery and formulation laboratory under the supervision of Prof. Leroux and received her Ph.D. in 2015. Her thesis was related to the chemical synthesis of biomolecules analogs. She joined the BioNanomaterial group at the Adolphe Merkle Institute in Fribourg, Switzerland, in 2015 as a postdoctoral researcher. Her current research interests focus on the synthesis of nanomaterial and the study of their toxicity under realistic conditions with a special focus on the 3D lung model.



Hana Barosova studied Nanotechnologies at Technical University of Ostrava, Czech Republic, where she received her M.Sc. in 2012. She joined Adolphe Merkle Institute in 2014 as Sciex-NMS fellow investigating the potential adverse effect of brake wear particles on the human epithelial cell

culture model, and in 2015 she started her Ph.D. Her research focuses mainly on the development of the human lung coculture model and its susceptibility to carbon-based materials.



Barbara Drasler studied Biology at the University of Ljubljana in Slovenia. She continued her studies there in the Nanobiology and Nanotoxicology research group and obtained a Ph.D. in Nanoscience and Nanobiology in 2014. In her dissertation, she tested and compared the effects of nanomaterials on

artificial and biological membranes. She joined the BioNanomaterials research group at the Adolphe Merkle Institute as a postdoctoral research fellow in 2016. Her main research interest has been directed toward the use of nanomaterials in medical field, particularly regarding their inherent safety when intentionally used within such applications, as well as concerning the occupational hazard of nanomaterials.



Laura Rodriguez-Lorenzo holds both Bachelor (2007) and Ph.D. (2012) degrees in Chemistry and Nanotechnology, respectively, from University of Vigo. Afterwards, she worked for 5 years in the BioNanomaterials group at the Adolphe Merkle Institute, Fribourg, Switzerland. She joined the Water Quality group in the

International Iberian Nanotechnology Laboratory in Braga, Portugal, in 2018 as Marie-Curie researcher. Her present research interests mainly focus on real time monitoring of biotoxins and other organic pollutants in water, the synthesis of hybrid composites for photocatalytic water purification, nanoecotoxicology, and surface-enhanced spectroscopies.



Dominic A. Urban studied Chemistry with Material Science at the Karlsruhe Institute of Technology and the Bonn-Rhein-Sieg University of Applied Sciences and received his B.Sc. in 2009. He continued his studies at the Philipp University of Marburg, where he received his M.Sc. in Chemistry in

2012. His master thesis was on the topic of studying the application possibilities of Taylor-dispersion analysis as a characterization technique for nanoparticles. He joined the BioNanomaterials group in the Adolphe Merkle Institute at the University of Fribourg, Switzerland, in 2014 as a Ph.D. student. His research interests are nanoparticle characterization, in particular TDA, studying the interactions of nanomaterials with biological systems and studying the colloidal stability of nanoparticles in complex biological media.



Dimitri Vanhecke received his M.Sc. in Biology from the University of Ghent, Belgium. He then moved to the group of Dr. Daniel Student at the University of Bern, Switzerland. After his Ph.D. in Structural Biology (in 2005), he held positions in the group of Prof Matthias Ochs (Experimental

Anatomy, University of Bern, Switzerland) and Prof Baumeister (Molecular Structural Biology, Max Planck Institute of Biochemistry, Munich). In 2012, he joined the Adolphe Merkle Institute, Switzerland, as a senior scientist. His primary interests are the structure-function relationships in biological landscapes.



Dedy Septiadi studied Engineering Physics and Biophotonics at Institut Teknologi Sepuluh Nopember (Indonesia) and École normale supérieure de Cachan (France) for his undergraduate and Master's degrees, respectively. In 2015, he obtained his Ph.D. in Physical Chemistry under the supervision of Prof.

Luisa De Cola at the University of Strasbourg (France). Since 2016, he has been a postdoctoral researcher at the Adolphe Merkle Institute (Switzerland) working with Prof. Barbara Rothen-Rutishauser and Prof. Alke Fink. His research interests are in the fields of bioimaging, cell mechanics, and nanomedicine.



Liliane Hirschi-Ackermann finished her apprenticeship for chemical labs in 1987 in a Swiss chemical company. She was then working for several chemical companies in Switzerland for 22 years, where she gathered extensive experience of particle synthesis and their characterization. She has joined

Adolphe Merkle Institute in 2009 focusing on synthesis and characterization of colloids. Recently, she synthesizes a broad spectrum of nanomaterials and provides the support to BioNanomaterials group researchers.



Alke Petri-Fink received her Ph.D. in Chemistry from the University of Ulm, Germany, in 1999. After a postdoctoral stay at the University of Gainesville, Florida, she joined the Institute of Materials Science at the école Polytechnique Fédérale de Lausanne (EPFL), first as a postdoctoral researcher,

then as a senior scientist. She became an Associate Swiss National Science Foundation Professor in the Department of Chemistry at the University of Fribourg in 2009, and full professor in 2011 at the Adolphe Merkle Institute, Switzerland, as the co-chair in BioNanomaterials. Her research focuses on inorganic nanoparticles, their synthesis, surfaces, and interactions with biological cells.



Barbara Rothen-Rutishauser has received her Ph.D. in 1996 in Cell Biology at the Swiss Federal Institute of Technology (ETH) in Zurich. From 1996 to 2000, she held a postdoctoral position in Biopharmacy at the Institute of Pharmaceutical Sciences at the ETH and in 2000 she joined Prof. Peter

Gehr's research group at the University of Bern, Switzerland, as a postdoc. After promotion to group leader in 2006, she

completed her habilitation in Cell Biology in 2009. Since 2011, she is the new co-chair in BioNanomaterials at the Adolphe Merkle Institute, University of Fribourg, Switzerland; the position is shared equally with Prof. Alke Petri-Fink. She has published more than 200 peer-reviewed papers and is an associate editor of the journal *Particle and Fibre Toxicology*. She is an expert in the field of cell-nanoparticle interactions in the lung, with a special focus on 3D lung cell models and various microscopy techniques such as laser scanning and transmission electron microscopy.

Prof. Rothen-Rutishauser and Prof. Petri-Fink share a full professorship in BioNanomaterials. This opportunity has many benefits, such as shared responsibility for challenging leadership tasks and more time for the families. The job-sharing also has the special feature that two scientific competencies are combined—namely, cell biology and materials science—which gives new insights and opportunities into the field of research. Accordingly, the research group is also a colorful mixture of various scientific disciplines, such as chemistry, material science, biochemistry, biology, physics, microscopy, hazard assessment, and environmental and food sciences. Such a constellation requires a lot of energy, open-mindedness, and respect for the other. Close cooperation and great trust of the two chairs in each other is a prerequisite for a successful job-sharing, but also the employees have to accept two supervisors and the colleagues in the Institute and the Faculty two opinions—until now the reactions, acceptance, and experiences on this job-sharing model are without exception very positive. What did it require to create such a special situation? First, it took some courage to apply together—according to the motto “together or not at all”—and fortunately the members of the search committee, the Faculty as well as the Rectorate in Fribourg were always positive and supportive. Second, the private environment was enormously encouraging and the advice “find the right partner” should also inspire younger researchers since this is highly relevant for an academic career.